OFFICE OF NAVAL RESEARCH

Contract N00014-94-1-0323

R&T Code 413v001

Technical Report No. 4

THE ROLE OF REDOX CHEMISTRY IN SCANNING TUNNELING MICROSCOPY IMAGING OF ELECTROACTIVE FILMS

by

Shelly R. Snyder and Henry S. White

Submitted for publication

Journal of Electroanalytical Chemistry

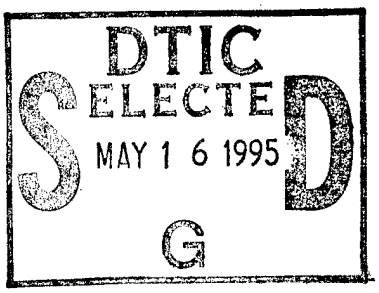

University of Utah
Department of Chemistry
Salt Lake City, UT 84112

April 31, 1995

REPORT DOCUMENTATION PAGE

Form Approved
OMB No. 0704-0188

1. AGENCY USE ONLY (Leave blank)	2. REPORT DATE	3. REPORT TYPE AND DATES COVERED
	3/31/95	Interim 6/94 - 12/94

4. TITLE AND SUBTITLE
The Role of Redox Chemistry in Scanning Tunneling Microscopy Imaging of Electroactive Films

5. FUNDING NUMBERS
N0014-94-1-0323

R & T Code 413V001

6. AUTHOR(S)
Shelly R. Snyder and Henry S. White

7. PERFORMING ORGANIZATION NAME(S) AND ADDRESS(ES)
Department of Chemistry
Henry Eyring Building
University of Utah
Salt Lake City, Utah 84112

8. PERFORMING ORGANIZATION REPORT NUMBER
4

9. SPONSORING/MONITORING AGENCY NAME(S) AND ADDRESS(ES)
Office of Naval Research
800 North Quincy Street
Arlington, Virginia

10. SPONSORING/MONITORING AGENCY REPORT NUMBER

11. SUPPLEMENTARY NOTES

12a. DISTRIBUTION/AVAILABILITY STATEMENT
Unclassified/Unlimited

12b. DISTRIBUTION CODE

13. ABSTRACT (Maximum 200 words)

The dependence of tunneling current (i) on bias voltage (V_b) in scanning tunneling microscopy (STM) measurements of multilayer electroactive films is interpreted in terms of a redox mechanism involving electron-transfer reactions at the STM tip/film and electrode/film interfaces. Analysis suggests that a symmetrical i-V_b response is anticipated when the molecular film is sufficiently thick (~2 - 3 monolayers) that the electron-transfer steps at the STM tip and electrode can be considered as discrete steps in the current-carrying processes. A macroscopic, two-electrode, thin-layer electrochemical cell is used to mimic the response of an electrode/redox film/STM tip junction. Steady-state, symmetrical i-V responses are obtained for the thin-layer cell, even when the solution initially contains only one-half of an electroactive redox couple. Tunneling spectroscopic measurements, using a STM, of dry films of protoporphyrin(IX)Fe(III)Cl deposited on highly oriented pyrolytic graphite electrodes are interpreted in terms of the proposed redox mechanism.

14. SUBJECT TERMS

15. NUMBER OF PAGES

16. PRICE CODE

17. SECURITY CLASSIFICATION OF REPORT	18. SECURITY CLASSIFICATION OF THIS PAGE	19. SECURITY CLASSIFICATION OF ABSTRACT	20. LIMITATION OF ABSTRACT
Unclassified	Unclassified	Unclassified	

THE ROLE OF REDOX CHEMISTRY IN SCANNING TUNNELING MICROSCOPY IMAGING OF ELECTROACTIVE FILMS

Shelly R.Snyder
Department. of Chemistry and Biochemistry, University of Texas
Austin, TX 78712

and

Henry S. White*
Department of Chemistry, University of Utah
Salt Lake City, UT 84112

ABSTRACT. The dependence of tunneling current (i) on bias voltage (V_b) in scanning tunneling microscopy (STM) measurements of multilayer electroactive films is interpreted in terms of a redox mechanism involving electron-transfer reactions at the STM tip/film and electrode/film interfaces. Analysis suggests that a symmetrical i-V_b response is anticipated when the molecular film is sufficiently thick (~2 - 3 monolayers) that the electron-transfer steps at the STM tip and electrode can be considered as discrete steps in the current-carrying processes. A macroscopic, two-electrode, thin-layer electrochemical cell is used to mimic the response of an electrode/redox film/STM tip junction. Steady-state, symmetrical i-V responses are obtained for the thin-layer cell, even when the solution initially contains only one-half of an electroactive redox couple. Tunneling spectroscopic measurements, using a STM, of dry films of protoporphyrin(IX)Fe(III)Cl deposited on highly oriented pyrolytic graphite electrodes are interpreted in terms of the proposed redox mechanism.

*To whom correspondence should be sent.
Submitted to *J. Electroanalytical Chem.*, Dec., 1994; revised March, 1995.

INTRODUCTION

Electron tunneling processes that occur during scanning tunneling microscopy (STM) imaging of *thin films* of electroactive molecules have, in principle, a similar basis as electron-transfer reactions that occur in conventional electrochemical reactions [1, 2]. In the conventional electrochemical experiment, electron-transfer occurs between a metal surface and an electroactive molecule (within a layer of solvent molecules and ions which create the electrical double layer at the solvent substrate interface). In the STM imaging of electroactive films, electron-transfer occurs between a metal tip and the substrate coated with a molecular adsorbate and associated counterions. The conceptual similarity of these two processes has been exploited by Morisaki and co-workers [3-5] in using thin SiO_2 tunnel barriers (on macroscopic Pt silicide substrates) in tunneling spectroscopy (TS) experiments [6] designated to probe the electronic density of states (DOS) of electrochemical molecules. An important difference between the study of electron-transfer reactions in TS experiments and in conventional electrochemical measurements is that mass-transfer limitations may be expected to be absent (or less pronounced) during TS experiments due to the close proximity of the tip with the molecules and substrate. In principle, the removal of mass-transport limitations, which frequently obscure quantitative analyses of electron-transfer mechanisms, allows detailed investigations of the kinetics of very fast electron-transfer reactions, as recently demonstrated in several laboratories [7,8].

In this preliminary report, we present experimental observations of the dependence of the tunneling current (i) on the voltage (V_b), (measured in a conventional STM arrangement) across thin films of protoporphyrin(IX)Fe(III)Cl (>2 monolayers) deposited on highly-oriented pyrolytic graphite (HOPG) electrodes. In contrast to highly asymmetrical i-V_b tunneling responses observed for monolayers of atomic adsorbates on a metal (e.g., halogen atoms on Ag [9]), or for semiconducting oxide films [10], the observed i-V_b response for PP(IX)Fe(III)Cl films, and other thick redox films studied in

our laboratory, is symmetric about the voltage axis, the magnitude of tunneling current being independent of the direction of the applied bias. Examples of this behavior will be shown below for relatively thin (several monolayers) and thick (~50 nm) films of PP(IX)Fe(III)Cl deposited on graphite electrodes. Since the electron tunneling distances in these experiments are probably no greater than ~10Å, the flow of current between the STM tip and the underlying electrode must also involve transport of electrons within the electroactive film. Thus, these tunnel junctions, which we designate as STM tip/electroactive film/electrode, are physically and conceptually similar to the more well-studied thin-layer redox-polymer devices, in which an electroactive polymer (wet [11, 12] or dry [13]) is sandwiched between two macroscopic metal electrodes (i.e., electrode/electroactive film/electrode). In the latter devices, the observed i-V_b response is known to reflect diffusional transport of electrons within the electroactive film (i.e., electron-hopping), the rate of electron-transfer at the two electroactive film/electrode interfaces, and/or the initial concentrations of the reduced and oxidized halves of the redox system that comprises the electroactive film. A quantitative analysis of the i-V_b response the two-electrode thin-layer cell has been presented in the discussion of the performance of thin-layer polymer-based solar cells (e.g., n-CdS/polyvinylferrocene/Au) [14]. The key differences between the configurations of the STM tip/electroactive film/electrode junction and the electrode/electroactive film/electrode cells are: (1) the vast differences in the geometrical areas defining the interfacial contacts (10 to 100 $Å^2$ in the case of STM and 0.1 to 1 cm^2 in the case of the thin-layer cell), and (2) the thicknesses of electroactive films that can be employed in these two situations. In the STM measurement, the electroactive film may be molecularly thin; electroactive films employed in the macroscopic devices, however, are considerably thicker in order to avoid electrical shorts between the two exterior electrodes. These geometrical differences, however, do not obscure the similarities in the role that redox chemistry might play in determining the overall i-V_b behavior in STM and in macroscopic, thin-layer cells.

In this report, we experimentally demonstrate similarities in the i-V_b responses observed for a macroscopic 2-electrode thin layer cell containing a redox active species and that observed in tunneling spectroscopy experiments of PP(IX)Fe(III)Cl films. The results are used to rationalize the mechanism of electron conduction in STM imaging of redox-active films, and suggest a methodology for employing STM in measurements of ultra-fast electron-transfer kinetics.

EXPERIMENTAL.

Reagents. Protoporphyrin(IX)Fe(III)Cl (Fluka) and analytical grade sodium borate ($Na_2B_4O_7$, Mallinckrodt) were used as received. Water was purified (18MΩ) with a Water Prodigy apparatus (Labconco Corp.).

Instrumentation and Methods. STM images were obtained in air with a Nanoscope II (Digital Instruments). Images were recorded in constant current mode using scan rates ranging from 2.5 to 5.6 Hz. Tunneling tips were constructed from mechanically cut Pt(70%)-Rh(30%) wire. Bias voltages (V_b) and tunneling currents (i) varied for each image and are listed in the figure captions. Images are low-pass filtered. Tunneling spectroscopic (i vs V_b) curves were acquired at a constant tip-to-substrate separation by measuring the current between the tip and substrate while linearly scanning the voltage (with the tip-to-substrate bias voltage interrupted). Data were obtained for $V_b = \pm 1.5$ V over a 0.2 sec. interval for the adsorbed PP(IX)Fe(III)C1 films and for $V_b = \pm 2.0$ V over a 0.2 sec. interval for electrooxidized PP(IX)Fe(III)Cl films. Tunneling currents observed in the i-V_b measurements range from 1 to 50 nA. Each i-V_b plot is comprised of ~10^{10} electron-transfer events (plus or minus one order of magnitude).

Electrodes were prepared using a ~0.6 x 0.6 x 0.1 cm piece of highly oriented pyrolytic graphite, HOPG, (Grade A or Grade B, Union Carbide). Electrical contact to the back side of the HOPG sample was made with a copper wire and conductive epoxy (Epo-

tek H20E, Epoxy Technology, Inc.). The HOPG substrate was mounted perpendicular to the end of a glass tube with epoxy, exposing both the front basal plane and edges to the solution. Following adsorption or electropolymerization of PP(IX)Fe(III)Cl, electrodes were rinsed with water and air dried. The HOPG substrate was removed intact from the glass tube for STM measurements by inserting a razor blade between the substrate and the epoxy.

Voltammetric experiments were performed with a EG&G Princeton Applied Research Model 173 Potentiostat and a Model 175 Universal Programmer. The electrochemical cell consisted of a sodium saturated calomel reference electrode (SSCE), a platinum wire coil counter electrode and the HOPG working electrode. Dissolved oxygen was removed from the solution by purging with prepurified N_2 prior to experimentation (20 min.) and by maintaining a positive pressure of N_2 in the cell above the solution during voltammetric measurements.

The two-electrode thin-layer cell was constructed using a home-built scanning electrochemical microscope (SECM), described in detail elsewhere [15]. A polished 0.4 mm-diameter Pt disk electrode was positioned directly above and parallel to a second identical Pt electrode. The separation distance between the two Pt electrodes was manually constrolled using a micrometer screw.

RESULTS AND DISCUSSION

Electrochemistry and STM Images

PP(IX)Fe(III)Cl-coated HOPG electrodes were prepared by two different methods reported in the literature: (1) adsorption, yielding a molecularly-thin electroactive film and (2) electrooxidative polymerization, yielding a relatively thick film.

Molecular films of PP(IX)Fe(III)Cl were formed by adsorption onto HOPG following the procedure of Anson and co-workers [16]. A freshly cleaved HOPG

electrode was placed in 0.1 M $Na_2B_4O_7$ solution (pH ~10.0) containing ~0.5 mM PP(IX)Fe(III)Cl and the potential was cycled between 0.0 and -1.2 V vs SSCE.

This potential range encompasses the half-way potential for the one-electron metal localized reduction of PP(IX)Fe(III)Cl, $E_{1/2}$ ~ -0.52 V vs SSCE. A diffusion-limited voltammetric response corresponding to PP(IX)Fe(III)Cl reduction was observed during deposition.

Fig. 1 shows the cyclic voltammetric response of the HOPG electrode in an aqueous solution containing only $Na_2B_4O_7$ following adsorption of PP(IX)Fe(III)Cl. The voltammogram shows nearly symmetrical reduction and reoxidation waves of equal magnitude, consistent with reversible electron-transfer between the surface-bound redox species and HOPG. The surface coverage of PP(IX)Fe(III)Cl on the basal plane of HOPG, Γ, estimated from the voltammetric response is ~1 x 10^{-10} mol/cm^2. This value corresponds to an average film thickness of ~2-3 monolayers based on the molecular dimensions of PP(IX)Fe(III)Cl (~14 x 17 Å^2) [17, 18] and assuming that PP(IX)Fe(III)Cl. is adsorbed in a closed-packed array with its planar face parallel to the electrode surface.

Thick films of PP(IX)Fe(III)Cl were prepared by oxidative electropolymerization using the method of Macor and Spiro [19]. A freshly-cleaved HOPG electrode was placed in a 0.1 M sodium borate solution (pH ~ 10.0) containing ~0.5 mM PP(IX)Fe(III)Cl, and the potential was cycled between 0.0 and +1.0 V vs SSCE. The polymer film results from radical vinyl coupling of PP(IX)Fe(III)Cl at E_p ~0.36 V; however, at potentials slightly positive of the value, PP(IX)Fe(III)Cl also slowly undergoes a 6-electron reduction to an electrochemically-inert quinoidal dioxoporphomethane species in aqueous solutions [20]. Thus, the films prepared by this method are comprised contain both electroactive PP(IX)Fe(III)Cl and electroinactive molecules. A voltammetric wave corresponding to the metal-centered 1-e- reduction of polymeric PP(IX)Fe(III)Cl was observed in aqueous solution containing only $Na_2B_4O_7$. The shape of the wave and the value of $E_{1/2}$ are similar to that shown in Fig 1, indicating that a significant fraction of the PP(IX)Fe(III)Cl

remains intact. The thickness of the film was estimated to be ~50 nm, based on in-situ quartz crystal microbalance measurements of the mass deposited during electropolymerization [21].

Fig. 2 shows representative STM images of adsorbed and electropolymerized PP(IX)Fe(III)Cl films. The structures observed in Fig. 2a for adsorbed PP(IX)Fe(III)Cl show what appear to be ~50 Å-diameter aggregates, consistent with the known tendency of PP(IX)Fe(III)Cl to form aggregates in aqueous solution. In contrast, oxidative electropolymerization yields a more densely-packed film comprised of polymerized clusters. A detailed analysis of the film structure will be presented elsewhere [21]. For the purpose of the present report, the key observation to be made from Fig. 2 is that the films appear to be continuous over large areas of the electrode surface. For comparison, Fig. 3 shows an image of the bare HOPG substrate prior to deposition of PP(IX)Fe(III)Cl.

Current-Voltage Behavior

Our discussion of electron transfer reactions that may occur during STM imaging is focused on electroactive molecular films that undergo chemically reversible and facile electron-transfer reactions of the type $O + ne^- \rightarrow R$ at a conducting substrate. The reversible metal-centered reduction of PP(IX)Fe(III)Cl (i.e., PP(IX)Fe(III)Cl + $e^- \rightarrow$ PP(IX)Fe(II)Cl), evident in the voltammetric response shown in Fig. 1, is a typical example of this class of reactions.

To explore the mechanism of STM imaging of PP(IX)Fe(III)Cl films, the tunneling current (i) as a function of bias voltage (V_b) curves were measured while holding the STM tip at a constant position (x,y,z) above the electrode. Prior to recording the i-V_b reponse, the HOPG/PP(IX)Fe(III)Cl electrodes were removed from the 0.1 M $Na_2B_4O_7$ solution at 0.0 V vs SSCE (corresponding to the fully oxidized Fe(III) state), washed with distilled H_20 and air dried. Fig. 4a shows i-V_b data that were obtained for an adsorbed film of PP(IX)Fe(III)Cl (corresponding to the image in Fig. 2a). It is evident that the i-V_b curve

is symmetric about the voltage axis, with equal current magnitude at negative and positive values of V_b. In addition, the tunneling current reaches a quasi-limiting value at biases larger than ca. 1.0 V.

Fig. 4b shows the i-V_b response for molecular films derived by oxidative electropolymerization of PP(IX)Fe(III)Cl. In contrast to the i-V_b curve for adsorbed PP(IX)Fe(III)Cl on HOPG, the tunneling current for this electrode increases nearly exponentially at large positive and negative biases ($> \pm$ 0.75 V), defining a region in which the current is relatively small and constant. However, the i-V_b response is again symmetric about the voltage axis.

The curves shown in Figs. 4a and 4b are representative of numerous measurements in which a symmetrical i-V_b dependence is observed. The magnitude of the current and shape of the i-V_b curves varied considerably from one measurement to another. We believe that this lack of reproducibility is due to the tip probing different regions of the films, as well as to differences in the separation distance between the STM tip and film-covered electrode. However, the symmetric waveshape, which is the focus of this report, is a constant feature in all of the i-V_b curves.

For comparison to the measurements on the PP(IX)Fe(III)Cl-coated electrodes, Fig. 4c shows the i-V_b curve obtained on the basal plane of bare HOPG. The shape of this i-V_b curve is in good agreement with previous literature reports [22]. The slight nonlinearity in the i-V curve is due to an increase in the surface density of states at energies slightly removed from the Fermi level of the substrate.

We propose that the general shape of i-V_b plots measured for both adsorbed polymerized PP(IX)Fe(III)Cl films on HOPG can be accounted for by assuming that the overall electron transfer mechanism between the STM tip and the underlying HOPG substrate occurs via a charge transfer mechanism, mediated by adsorbed PP(IX)Fe(III)Cl:

$$PP(IX)Fe(III)Cl + e^-_{tip} \rightarrow PP(IX)Fe(II)Cl \qquad (1)$$

$$PP(IX)Fe(II)Cl + PP(IX)Fe(III)Cl \rightarrow PP(IX)Fe(III)Cl + PP(IX)Fe(II)Cl \quad (2)$$

$$PP(IX)Fe(II)Cl \rightarrow PP(IX)Fe(III)Cl + e^-_{HOPG} \quad (3)$$

The subscripts "tip" and "HOPG" indicate the location of the transferring electron. Eq. 2 represents the transport of electrons within the film, via a homogeneous electron transfer reaction between Fe(II) and Fe(III) states. The viability of redox-active films to conduct electrons by such a exchange mechanism has been established in many laboratories. Eqs. 1 and 3 are assumed to be reversible, allowing tunneling currents of equal magnitude to be observed at both positive and negative biases as is experimentally observed. An implicit assumption in proposing a redox mechanism is that the molecular film is weakly coupled with the electronic states of the substrate and tip, as is qualitatively depicted in Fig. 5, and that the film is sufficiently thick that direct tunneling between the tip and substrate is unlikely. We note that a conceptually similar mechanism (without electron transport, eq. 2) is implicit in recent models proposed by Gimzewski and co-workers in their analysis of the contrast on STM images of monolayers of copper phthalocyanine [23] and by Zheng and Tsong in their analysis of resonant tunneling via tip-localized, molecular electron traps [24].

The symmetrical i-V_b response suggests that both oxidized (PP(IX)Fe(III)C1) and reduced (PP(IX)Fe(II)Cl) forms of the adsorbed electroactive film participate in the tunneling processes, although only PP(IX)Fe(III)Cl is initially present in the as-formed film upon removal of the electrode from solution at 0.0 V vs SSCE. This apparent inconsistency can be removed by noting that the STM tip is probing a very small absolute number of redox molecules whose redox distribution (i.e., the ratio of oxidized and reduced sites, PP(IX)Fe(III)Cl/(PP(IX)Fe(II)Cl) will be effected by the sign and magnitude of the potential applied between the tip and HOPG substrate. For instance,

assuming that the STM tip is biased at a large negative value, electrons will initially be transferred from the tip to PP(IX)Fe(III)Cl (eq. 1), yielding PP(IX)Fe(II)Cl at the tip/film interface. Once generated, the reduced porphyrin at this interface may be reoxidized by the electron-exchange reaction (eq. (2)), leading to propagation of charge across the film to the HOPG/film interface. The magnitudes of the electron-transfer rate constants of eqs. 1 and 3, and the rate of electron-exchange, eq. 2, will determine which of the microscopic steps will limit the overall flux of electrons from the tip to the substrate. Conversely, at large positive tip-to-HOPG biases, electron flow will occur by the reduction of PP(IX)Fe(III)Cl via electron-tunneling from HOPG to the adsorbed layer (the reverse direction of eq. 3), followed by charge transport (eq. (2)) and reoxidation of PP(IX)Fe(II)Cl by the tip (the reverse direction of eq. 1).

The above arguments indicate that the adsorbed electroactive film, as removed from the electrochemical cell in the fully oxidized Fe(III) state, functions as both acceptor and donor states in the electron-tunneling processes, mediating the current between the STM tip and HOPG substrate at both positive and negative biases. The ability of *one half* of a redox-acitve couple to act as the charge carrying species at both positive and negative bias is somewhat surprising but can be readily demonstrated in a more conventional electrochemical experiment employing a 2-electrode thin-layer cell (TLC) in which only one-half of a soluble redox couple is initially present in the solution. For example, Fig. 6 shows the cyclic voltammetric response of a 0.4 mm radius Pt electrode (employing a 3-electrode cell arrangement with reference and auxillary electrodes) in a bulk solution of 10 mM $K_4Fe(CN)_6$ containing 0.1 M Na_2SO_4 as supporting electrolyte. A voltammetric wave centered at the half-wave potential of the $Fe(CN)_6^{-3/-4}$ couple, $E_{1/2}$ = 0.19 V vs. SSCE, is observed when the electrode potential is initially scanned to positive values, corresponding to the oxidation of $Fe(CN)_6^{-4}$ and re-reduction of electrogenerated $Fe(CN)_6^{-3}$. When the potential is scanned to negative values, a cathodic current at ~-0.7 V vs. SSCE is observed which corresponds to the reduction of H_20 (E^o = -0.66 V vs. SSCE at pH 7). When the

same electrode is employed in a 2-electrode TLC, as one of two identical and closely spaced plane parallel Pt electrodes (see schematic in Fig. 6), the i-V behavior of the cell is a complex function of separation distance, d, between the two electrodes. In this experiment, a voltage is simply applied between the two electrodes, without controlling the potential of either electrode versus a reference electrode (completely analogous to the arrangement used in the STM measurements). At large separation distances, d = 200 μm, a peak-shaped i-V wave is observed, Fig. 6b, that has a shape qualitatively similar to the voltammetric wave observed at an individual Pt electrode in the 3-electrode cell, Fig. 6a. However, there are three significant differences in the response. First, the positive branch of the wave is largely suppressed on the initial positive-going scan (the 1st scan is indicated with an arrow). This occurs due to the fact that, at low biases (i.e., near 0 V), there is essentially no reducible species initially present in the solution necessary to balance the current at the second electrode. Since the most easily reduced species initially present in the solution is H_20 (see Fig. 6a), the minimum applied bias necessary to concurrently carry out *faradaic* processes at both electrodes is equal to $\{E^{0'}(Fe(CN)_6^{-3/-4}) - E^{0'}(H_20/H_2)\} \sim$ 0.9 V, significantly larger than the voltage range scanned in obtaining the voltammetric response shown in Fig. 6b. On the return scan, a peaked diffusion-limited wave is observed and, within 2 to 3 scans, a steady-state peaked shaped i-V response is obtained. The appearence of the peaked-shaped wave following the initial scan is undoubtedly due to the build-up of some $Fe(CN)_6^{-3}$ in the solution that results from oxidation of $Fe(CN)_6^{-4}$ at the positive electrode during the initial scan, accompanied by either double-layer charging of the negative electrode or reduction of solution impurities. The second point to note is that the magnitude of the peak currents are about an order of magnitude smaller in the 2-electrode TLC due than in the conventional 3-electrode cell (compare Figs. 6a and 6b). This is related to the fact that the overall response of the 2-electrode cell may be limited by diffusional transport of either $Fe(CN)_6^{-4}$ or $Fe(CN)_6^{-3}$, and specifically by whichever species is present at a lower concentration. For the experiment presented here, the

electrogenerated product, $Fe(CN)_6^{-3}$, is certainly present in the solution between the electrodes at a much lower concentration that the initial reactant, $Fe(CN)_6^{-4}$. Thus, it follows that the peak-shaped i-V response is due to diffusion and reduction of the product, $Fe(CN)_6^{-3}$, at either electrode, whenever that electrode is negative with respect to the second electrode. (It is important to realize here that the peak-shaped voltammetric response does not result from the conventional oxidation and re-reduction of reactanct, $Fe(CN)_6^{-4}$, at an individual electrode, as occurs in the 3-electrode arrangement employing a reference and counter electrode, Fig. 6a.) Comparing the peak currents in Figs. 6a and 6b, we estimate that $Fe(CN)_6^{-3}$ respresents about 10% of the total redox concentration within the gap separating the 2 electrodes. The third and final point to note is that the i-V wave is centered at 0.0 V applied bias (as opposed to 0.19 V in the 3-electrode potentiostatic arrangement). This shift obviously results from equilibration of the two Pt electrodes with bulk $Fe(CN)_6^{-4}$ (initally present in the solution) and with the product, $Fe(CN)_6^{-3}$, electrogenerated during the initial scans.

When the separation distance between the two Pt electrodes is decreased to ~10 μm. Fig. 6c, a true steady-state, sigmoidally-shaped i-V response is observed which displays well-defined, transport-limited current plateaus at both positive and negative biases. The symmetry and steady-state characteristics of this wave now reflect the fact that $Fe(CN)_6^{-4}$ oxidation at one electrode is balanced by an equal rate of $Fe(CN)_6^{-3}$ reduction at the opposite electrode. $Fe(CN)_6^{-3}$, which is not initially present in the solution, is electrogenerated and rapidly transported across the cell gap on the slow time-scales of these measurements. The steady-state sigmoidal-shaped response resulting from this mechanism is qualitatively similar to that discussed in context of twin-electrode cells (albeit under potentiostatic control) [25,26] and in applications of scanning elecrochemical microscopy [27].

The 2-electrode TLC with only one half of a redox couple present in solution is completely analogous to the STM tip/PP(IX)Fe(III)Cl/HOPG tunnel junction, with the

assumption that the PP(IX)Fe(III)Cl film is sufficiently thick to prevent direct tunneling between tip and HOPG substrate. Since the mass transport rates of $Fe(CN)_6^{-4}$ and $Fe(CN)_6^{-3}$ in the 2-electrode TLC are inversely proportional to the inter-electrode separation distance, d, the i-V_b response at sufficiently small values of d may eventually be limited by the heterogeneous electron-transfer reactions at the Pt electrodes (i.e., $Fe(CN)_6^{-3} + e^- \Leftrightarrow Fe(CN)_6^{-4}$). This point is addressed more quantitatively below. The key findings of the TLC experiment are: (i) steady-state currents of exactly equal magnitudes flow through the cell in both negative and positive biases when only one half of a reversible redox couple is *initially* present in the solution layer separating two closely spaced electrodes, and (ii) the two Pt electrodes and the redox potential of the solution ($E_{1/2}$) are rapidly equilibrated as evidenced by the symmetry of the wave around zero bias (0.0 V). These same features are observed in the i-V_b curves of the STM tip/PP(IX)Fe(III)Cl/HOPG junction (Fig. 5a), demonstrating the *feasibility* of eqs. 1 through 3 as the charge conduction mechanism in the STM experiment.

While the i-V measurements do not allow identification of eqs. 1, 2 or 3 as the rate-limiting step in the overall conduction mechanism, it is instructive to recast values of the tunneling current, i, as an apparent first order electron-transfer rate constant, k_{et} (s^{-1}). This can be accomplished by defining a geometrical area of the electroactive film that encompasses the tunneling region, A_T, and using the relationship

$$i = nFA_T\Gamma(\pm V_b)k_{et} \qquad (4)$$

In eq. (4), n is the number of electrons transferred per molecule (=1), F is the Faraday, and $\Gamma(\pm V_b)$ is the bias-dependent surface density (mol/cm^2) of electroactive molecules (ox or red) that can either act as electron acceptors (at negative tip-to-substrate bias) or donors (at positive tip-to-substrate bias). Approximating $\Gamma(\pm V_b)$ as equal to the total surface coverage of electroactive molecules, eq. (4) reduces to

$$I = nFA_T\Gamma k_{et} \qquad (5)$$

from which k_{et} can be readily experimentally evaluated from the tunneling current and the coulometric measurements of Γ.

To estimate k_{et} using eq. (5), we assume that electron-tunneling between the tip and substrate occurs within a circular region of area $A_T = \pi a^2$ where a is determined by the tip radius. Estimated values of the radius in the literature range from 5 - 20 Å [28] yielding A_T between 1 and 10 x 10^{-14} cm^2. We also assume that the electroactive film has a thickness d_f that is sufficiently small that charge introduced into the film as a result of a redox process (eqs. 1 or 3) is transported through the film in the direction normal to the substrate (while retaining the initial criterion of our analysis that the film is sufficiently thick that direct electron tunneling between the tip and substrate is negligible). This condition is fulfilled when $a >> d_f$. For the films of adsorbed PP(IX)Fe(III)Cl, a is of the order of d_f and some charge may leak outside the boundary defined by a, a complexity that we shall ignore.

Fig. 7 shows k_{et} values obtained using eq. 5 and the i–V_b data in Fig. 4a for an adsorbed PP(IX)Fe(III)Cl film. In calculating k_{et}, we assume Γ is equal to the electrochemically measured surface coverage (10^{-10} mol/cm^2) and $a \sim 20$Å. The data in Fig. 7 show that k_{et} increases from ~ 10^9 s^{-1} at zero bias (V = 0) to ~5 x 10^{10} s^{-1} at large positive or negative bias, $|V| \geq 0.7$ V. Due to the lack of quantiative reproducibility in the i-V_b response of the STM junction (noted above), these numbers are highly approximate. The dependence of k_{et} on V, however, can be qualitatively attributed to either a decrease in the activation energy for electron-transfer (eqs. 1 and 3) at large biases, or to an increase in the number of molecules that can act as donor and acceptor states at large positive and negative biases, respectively. As previously demonstrated for the case of the TLC cell initially containing only one half of a redox couple, the electroactive film directly beneath

the STM tip may be comprised of both oxidized and reduced states after a voltage is applied to the junction, the number density of each likely depending on bias voltage, V_b. To determine the functional dependence of $\Gamma(\pm V_b)$, however, would require a detailed kinetic model that relates k_{et} to the local electric potential, $\phi(x)$, at the interfaces and across the film. Since $\phi(x)$ is not known, the variation of $\Gamma(\pm V_b)$ with applied bias can not be readily determined. However, the symmetry of the i-V_b response suggests that the current is limited by the same species, regardless of the direction of current. Analogous to the interpretation of the TLC experiment, we propose that the response is limited by reactions involving the species with the smaller number density.

The observed dependence of k_{et} on V_b closely resembles the functional dependence of homogeneous electron-transfer rate constants on reaction free energy change (ΔG^o) [29,30]. Because of the complex potential distribution within the tunnel region, however, the applied bias is not necessarily equal to ΔG^o nor can it be ascertained if a strict linear proportionality exists between the two quantities. However, since it is obvious that the driving force for electron transfer increases with increasing bias, Fig. 7 is indeed a qualitative form of a free energy correlation.

As a final comment, in the analysis of the i-V_b response we have also quantitatively considered the rate of diffusional electron conduction within PP(I X)Fe(III)Cl films. For a film of thickness d_f and cross-sectional area A_T, the maximum diffusional flux is given by [31]

$$i = nFA_T D_{e^-} \Gamma / d_f^2 \qquad (7)$$

where D_{e^-} is an apparent diffusion coefficient for electrons and the other symbols represent previously defined quantities. Using the maximum current of i in Fig. 4a, $d_f = 20$ Å, and $A_T = 3.1 \times 10^{-14}$, yields $D_{e^-} = 10^{-2}$ cm^2/s. This value is ~10^4 times larger than the largest diffusion constants reported for electron conduction in redox films [32], suggesting that

electron diffuson by a site-to-site hopping mechanism is not an appropriate description of transport processes within the film. This is not altogether surprising since a large electric field (~10^5 V/cm) exists between the tip and HOPG. The rate of electron transport in redox polymers may be significantly altered by such high-field strengths.

CONCLUSION. Our preliminary analysis of the electron-tunneling mechanism suggests that the redox reactions of thick PP(IX)Fe(III)Cl films may mediate the flux of electrons between the STM tip and substrate. Such a mechanism appears reasonable for relatively thick films (> greater than 2 monolayers) where direct tunneling between electronic states of the STM tip and underlying metal electrode are not permissible. It is interesting to note that the measured values of k_{et} (10^9 - $5x10^{10}$ s^{-1}) obtained in the tunneling measurements are of the same order of magnitude as recently reported values of the first-order rate constants for exothermic electron-transfer reactions between dissimilar electroactive molecules separated by a saturated hydrocarbon spacer. For instance, Jordan et al. obtained k_{et} values as large as 1.8×10^{10} s^{-1} from time-resolved fluorescence measurements for excited-state electron-transfer from zinc mesophenyloctamethylrin to a series of benzoquinones separated by a 10 Å-long rigid hydrocarbon spacer [33]. Similar experiments by Closs and Miller yielded comparable values of electron-transfer rate constants (10^9 s^{-1}) for rigidly spaced electron donor and acceptor pairs [34] . Although obvious physical and chemical differences exist between the mechanisms of electron transfer involved in the STM experiment and in the purely chemical systems, the conceptual similarity between these reactions and the order-of-magnitude agreement in the observed rates suggests that STM can be employed to investigate the dynamics of extremely fast electron transfer reactions.

ACKNOWLEDGMENT.

The authors gratefully acknowledge the assistance of E. R. Scott in preliminary TLC experiments. This work was supported by the Office of Naval Research.

REFERENCES.

1. J. K. Sass and J. K. Gimzewski, J. Electroanal. Chem., 251 (1988) 241.
2. G. Travaglini, M. Amrein, B. Michel, and H. Gross, in *Scanning Tunneling Microscopy*; R. J Behm, N. Garcia, and H. Rohrer, Eds. Kluwer Academic Publishers, Netherlands, 1990.
3. H. Morisaki, A. Nishikawa, H. Ono, and K. Yazawa, J. Electrochem. Soc., 137 (1990) 2759.
4. H. Morisaki, H. Ono, and K. Yazawa, J. Electrochem. Soc., 136 (1989) 1710.
5. H. Morisaki, H. Ono, and K. Yazawa, J. Electrochem. Soc., 135 (1988) 381.
6. A. J. Bennett, Electroanal. Chem., 60 (1975) 125.
7. H. Finklea and D. D. Hanshew, J. Am. Chem. Soc., 114 (1992) 3173.
8. C. E. D. Chidsey, Science, 251 (1991) 919.
9. J. H. Schott and H. S. White, J. Phys. Chem., 98 (1994) 297.
10. N. Casillas, S. R. Snyder, W. H. Smyrl, and H. S. White, J. Phys. Chem., 95 (1991) 7002.
11. C. E. D. Chidsey and R. W. Murray, Science, 231 (1986) 25.
12. P. G. Pickup and R. W. Murray, J. Electrochem. Soc., 131 (1984) 833.
13. J. C. Jerigan, C. E. D. Chidsey, and R. W. Murray, J. Am. Chem. Soc., 107 (1985) 2824.
14. M. P. Hagemeister and H. S. White, J. Phys. Chem., 91 (1987) 150.
15. E. R. Scott, H. S. White, and J. B. Phipps, Anal. Chem. , 65 (1993) 1537.
16. A. P. Brown, C. Koval, and F. C. Anson, J. Electroanal. Chem., 72 (1976) 379.
17. P. Bianco, L. Haladjian, and K. J. Draoui, Electroanal. Chem., 279 (1990) 305.
18. C. F. Kolpin and H. S. Swofford, Anal. Chem., 50 (1978) 916.
19. K. A. Macor and T. G. Spiro, J. Chem. Soc., 105 (1983) 5601.
20. K. A. Macor and T. G. Spiro, J. Electroanal. Chem., 163 (1984) 223.

21. S. R. Snyder and H. S. White, J. Phys. Chem, manuscript in preparation.

22. M. Kuwabara, D. R. Clarke, and D. A. Smith, Applied Phys. Lett. 56 (1990) 2396.

23. J. K. Gimzewski, E. Stoll, and R. R. Schjlittler, Surf. Sci., 181 (1987) 267.

24. N. J. Zheng and I. S. T. Tsong, Phys. Rev. B41 (1990) 2671.

25. C. N. Reilley, Rev. Pure and Appl. Chem., 18 (1968) 137.

26. L. B. Anderson and C. N. Reilley, J. Electroanal. Chem., 295 (1965) 205.

27. D. O. Wipf and A. J. Bard, J. ELectrochem. Soc. 138 (1991) 469.

28. R. J. Behm, in *Scanning Tunneling Microscopy and Related Methods*; R. J. Behm, N. Garcia, and H. Rohrer, Eds., Kluwer Academic Publishers; 1989; p 173.

29. R. Ballardini, G.Varani, M. T. Indelli, V.Scandolaa, and J. F. Balzani, J. Am. Chem. Soc., 100 (1978) 7219.

30. D. Behm and A. Weller, Isr. J. Chem., 8 (1970) 259.

31. E. F. Dalton, R. W. Murray, J. Phys. Chem., 95 (1991) 6383.

32. R. W.Murray in *Electroanalytical Chemistry* , Vol 14, A. J. Bard, Ed., Wiley, New York, 1984.

33. A. D. Jordan, B. A. Leland, P. M. Felker, A. H. Zewall, J. J. Hopfield, and P. B. Dervan, Nature, 327 (1987) 508.

34. G. L. Closs and J. R. Miller, J. Am. Chem. Soc., 106 (1984) 2047.

FIGURE CAPTIONS.

1. Cyclic voltammetric response of a HOPG/PP(IX)FeCl (adsorbed) electrode in a N_2-purged, 0.1 M $Na_2B_4O_7$ solution. Voltametric sweep rate = 50 mV/s.

2. STM images of PP(IX)FeCl films on HOPG: (a) adsorbed film (~2 monolayers) imaged at V_b = 0.1 V and i = 1.2 nA; (b) electropolymerized film (~50 nm thick) imaged at V_b = 0.22 V and i =0.54 nA.

3. STM image of a bare HOPG electrode at V_b = 0.12 V and i = 0.7 nA.

4. i vs. V_b curves for HOPG/PP(IX)FeCl electrodes prepared by (a) adsorption and (b) electropolymerization. Curve (c) shows the i-V_b response of a bare HOPG electrode. Set-point voltages and currents were: (a) -0.1 V and -1.43 nA; (b) -0.33 V and -0.54 nA; and (c) 0.40 V and 1.01 nA.

5. Schematic drawing of electron-transfer reactions (top) between HOPG/PP(IX)FeCl and the STM tip, and the corresponding electric potential diagram (bottom) showing the distribution of redox states within the tunnel juction.

6. (a) Cyclic voltammetric response of a 0.4 mm-radius Pt electrode in a 0.01 M $K_4Fe(CN)_6$ and 0.1 M Na_2SO_4 solution. i-V_b response of a 2-electrode thin-layer cell comprised of two identical Pt electrodes separated by (a) 200 μm and (c) 10 μm and containing the same solution as in (a). Scan rate: 100 mV/s in all cases. In (a), the potential V is measured against the SSCE. In (b) and (c), V represents the voltage applied between the two Pt electrodes.

7. Plot of electron-transfer rate constant (k_{et}, s^{-1}) as a function of the total potential applied bewteen the STM tip and HOPG/PP(IX)FeCl (adsorbed) electrode. Values of k_{et} are calculated from tunneling currents, I, using eq. (5). Open (o) and closed

circles (•) represent values measured at negative and positive biases (sample vs. tip), respectively.

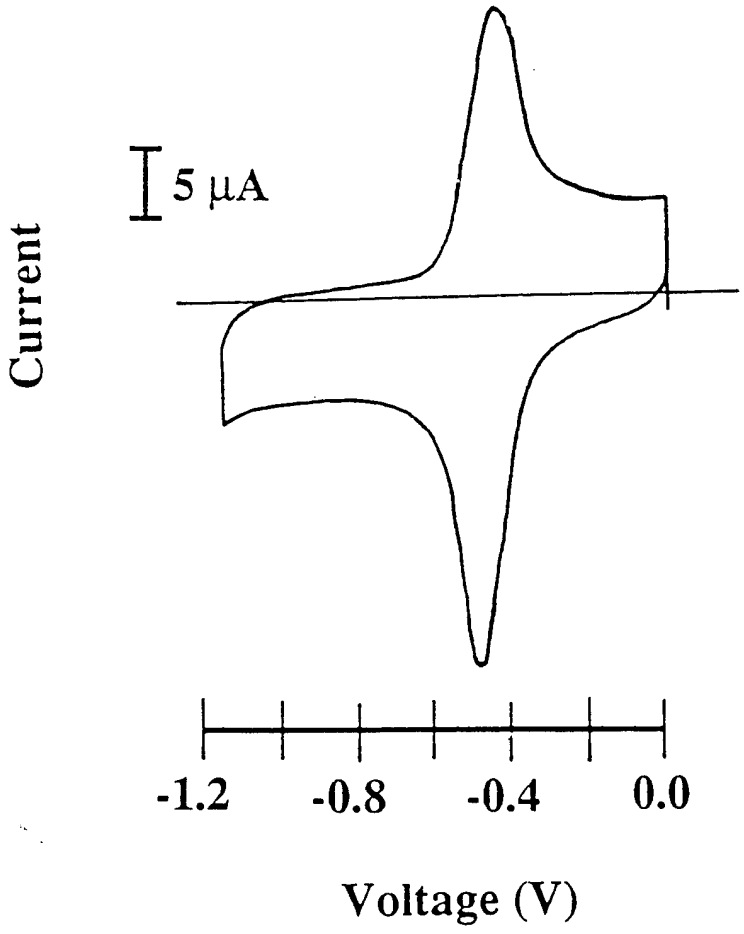

Fig 1

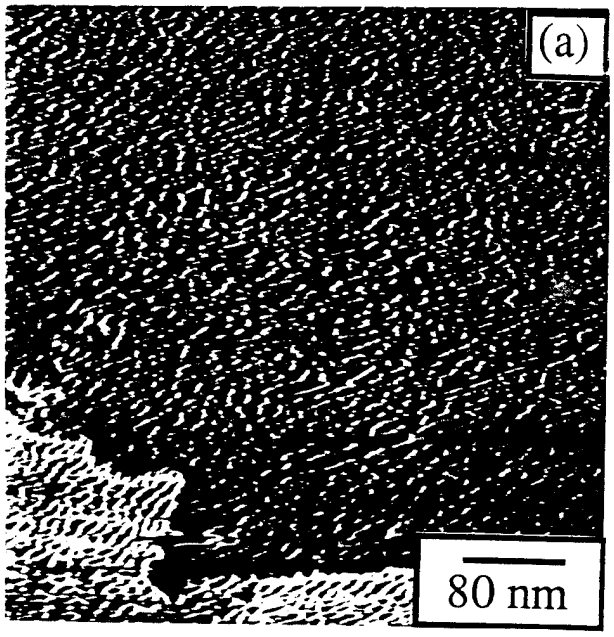

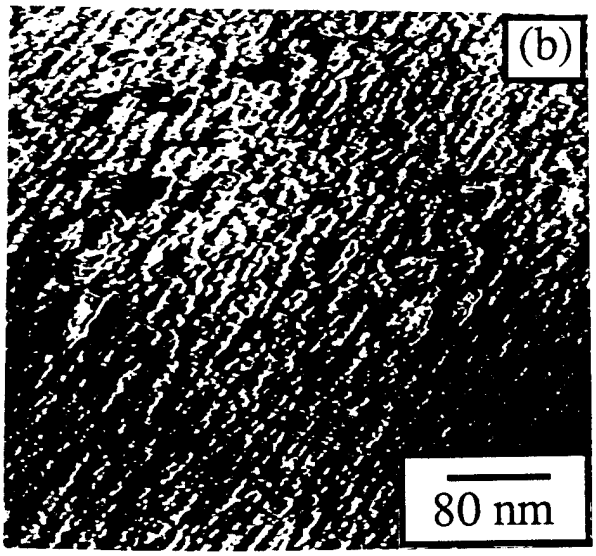

Fig. 2

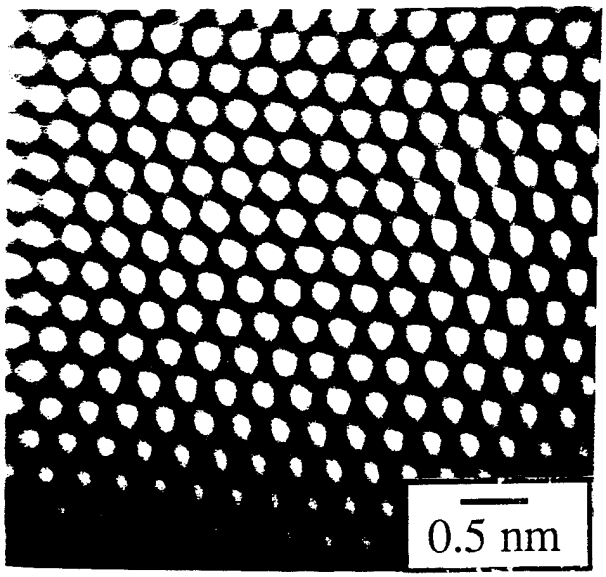

Fig. 3

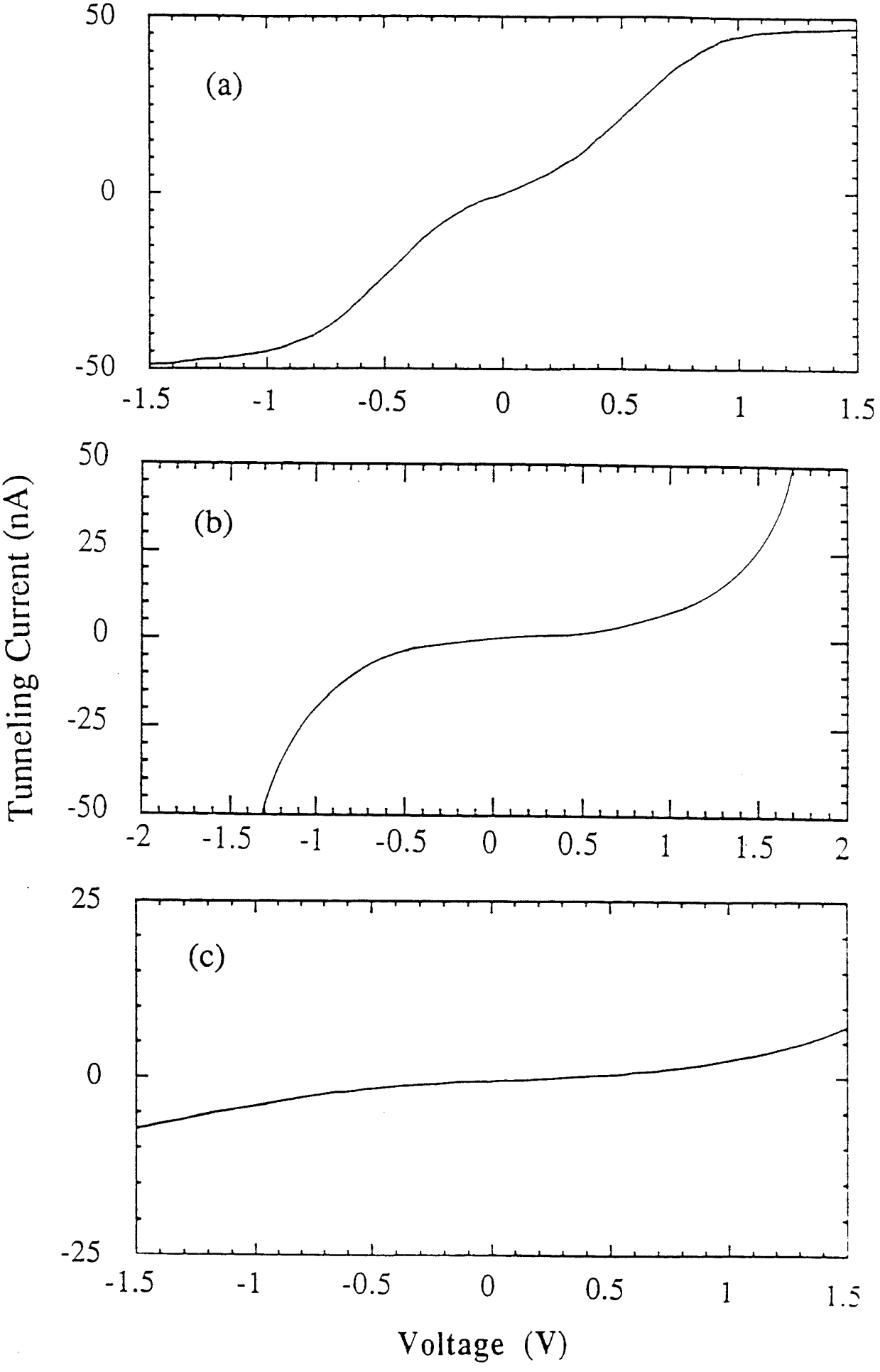
(a)
50
0
-50
-1.5
-1
-0.5
0
0.5
1
1.5
(b)
50
25
0
-25
-50
-2
-1.5
-1
-0.5
0
0.5
1
1.5
2
(c)
25
0
-25
-1.5
-1
-0.5
0
0.5
1
1.5
Tunneling Current (nA)
Voltage (V)

Fig 4

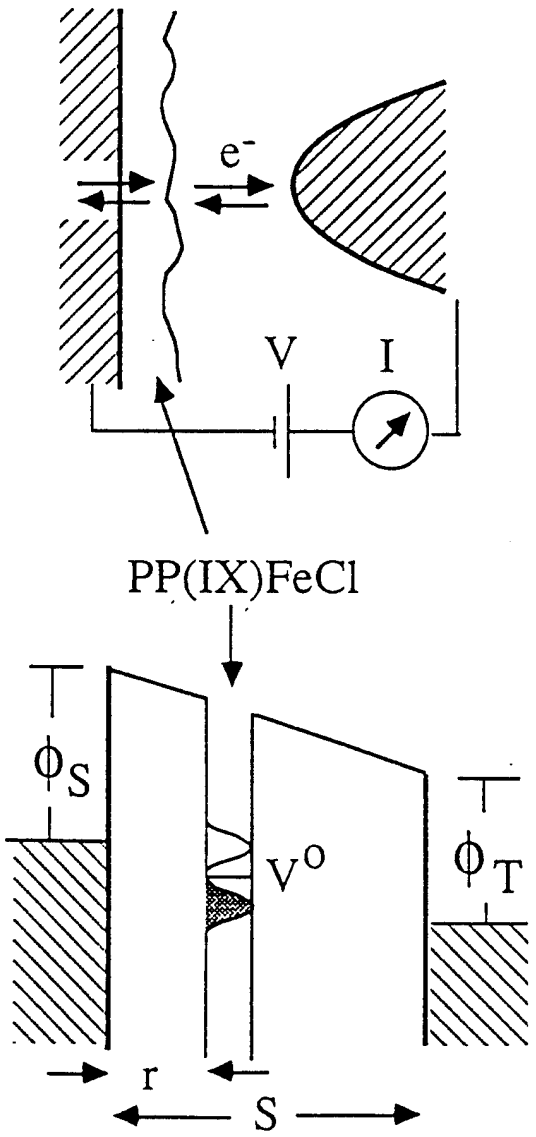

Fig 5